Figure 3. UV-Vis spectra of the gold ions source (HAuCl$_4$.3H$_2$O, yellowish color) and the synthesized gold nanoparticles (PAA-AuNPs, reddish-purple color) after chemical reduction process with their corresponding spherical shape (TEM image).

Once PAA-AuNPs have been synthesized with their characteristic reddish-purple coloration, the next step is to incorporate these nanoparticles into thin-films using the Layer-by-Layer Embedding (LbL-E) deposition technique. The use of PAA as an encapsulating agent of the nanoparticles plays a dual role. Firstly, it prevents the agglomeration or aggregation of the nanoparticles during the synthesis process. And secondly, this weak polyelectrolyte can be manipulated as a function of the pH in order to obtain ionized groups which are used to perform the multilayer assembly by the electrostatic attraction of oppositely charged polyelectrolytes. In this work, a pH 9.0 has been selected in order to fabricate the nanocoatings because it has been demonstrated that both polyelectrolytes at this pH value are totally ionized.

In Figure 4, the evolution of the transmitted spectra corresponding to [PAH(9.0)/PAA-AuNPs(9.0)]$_n$ at different number of bilayers is shown. The optical signal of the bare optical fiber was taken as reference for the absorption measurements during the fabrication process.
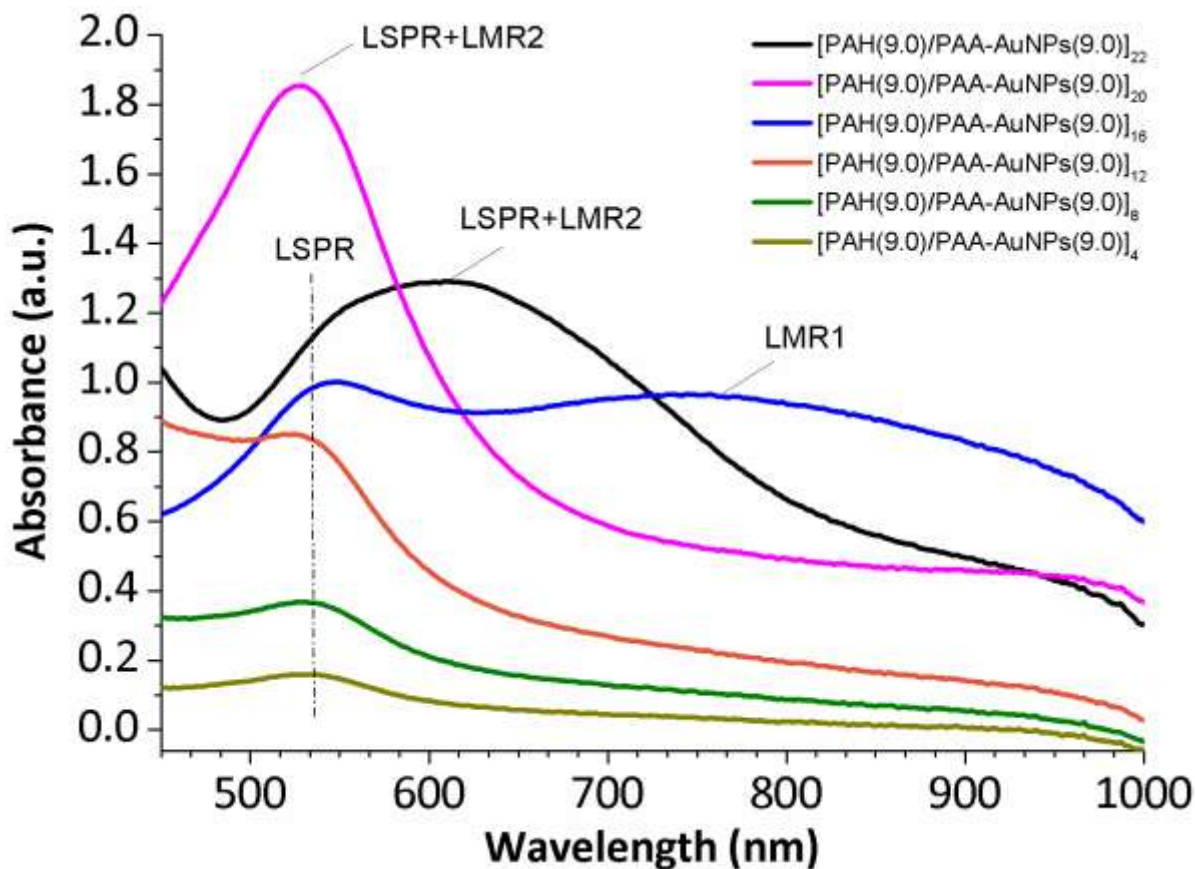

Figure 4. Transmitted absorption spectra during the deposition process from 1th to 22th bilayers. The curves plotted are 4, 8, 10, 12, 16, 20 and 22 bilayers.

Initially, when the thickness coatings is increased from 1 to 12 bilayers, only an absorption band centered at 530 nm is observed. This peak related to the LSPR phenomenon becomes higher as far the number of bilayers is increased, although it remains at the same wavelength position. Nevertheless, when the number of bilayers is increased up to 16 bilayers, two different resonant phenomena, LSPR and LMR1, are observed simultaneously in the visible spectra. The new LMR peak (LMR1) appears at low wavelengths and shifts to the right during the fabrication process. And finally, when thickness coating is increased up to 22 bilayers, the LMR1 peak exceeds the visible range and a new LMR band (LMR 2) is observed in the visible spectrum which is shifted

from shorter wavelengths to longer wavelengths as a function of the resultant thickness. This LMR2 peak can mask the LSPR peak when they are centered near it as it happens after 20 bilayers coating.

In order to characterize separately the response of the different resonances (LSPR, LMR1 and LMR2) to variations in the surrounding medium refractive index (SMRI), three different nanocoatings with different number of bilayers have been fabricated and characterized.

a. LSPR sensor (7-bilayers device)

The first device consisted of a coating with just 7 bilayers of [PAH(9.0)/PAA-AuNPs(9.0)] in which only the LSPR peak can be observed without any perturbations from LMR phenomena that could mask the signal. In Figure 5, it is shown the response of the LSPR band generated in this device when the sensitive coating is immersed into glycerin solutions with different SMRI.
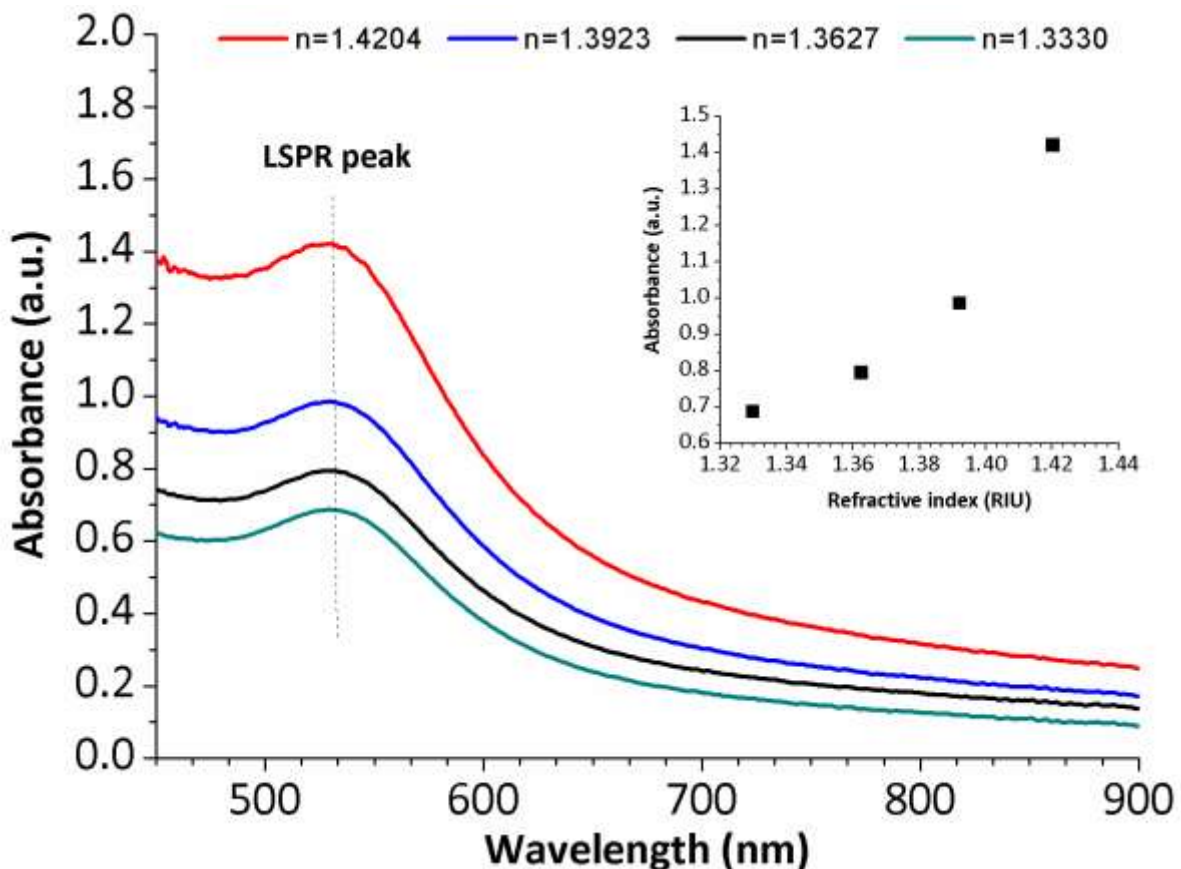

Figure 5. Spectral response of the LSPR absorption peak (7-bilayers device) and the evolution of the maximum absorbance of the LSPR band (inset) when the sensitive coating is immersed in different surrounding medium refractive indices (SMRI).

The results displayed in this Figure indicate that only a change in intensity of the LSPR absorption band is observed as SMRI is varied. As it can be clearly observed, the intensity of the LSPR absorption band increases as far as the SMRI becomes higher. In addition, no significant changes are observed in the wavelength position of the LSPR peak which it is perfectly centered at 530 nm after immersing the sensitive coating to different SMRI. In the inset of the Figure 5, the evolution of maxima absorbance of the LSPR absorption band is represented as a function of variable refractive index values from 1.33 to 1.4204.

b. LSPR-LMR sensor (16-bilayers device)

The second device was fabricated by depositing 16 bilayers of [PAH(9.0)/PAA-AuNPs(9.0)] in order toshow clearly both LSPR and LMR1 absorption bands in the spectral range. As it was observed in Figure 4, the LSPR absorption band is centered at 550 nm, whereas the LMR1 band is located around 750 nm.

In Figure 6, it is shown the red-shift of the LMR1 absorption band as SMRI is increased. In this same graph, it is possible to appreciate how the LSPR band shows no significant wavelength dependence with variable refractive index values because it is located between 540-550 nm and this aspect had been previously corroborated in the Figure 5. However, the LMR1 band shows a shift of 265 nm when the sensitive region is immersed in water solutions of glycerin with refractive index values from 1.3330 to 1.3627. In addition, a higher value of the refractive index (n>1.3627) makes the LMR1 band to be already out of the scope for this wavelength visible range. The LMR1 absorption band shows a very broad absorption peak with a high sensitivity of 8922 nm/RIU. This aspect has been experimentally proved in previous works [20] where it can be observed for polymeric films that the first LMR (LMR 1) shows a higher spectral width than the higher order LMRs. Due to this a study in higher order LMR has been performed in this work and it is shown in the following section.
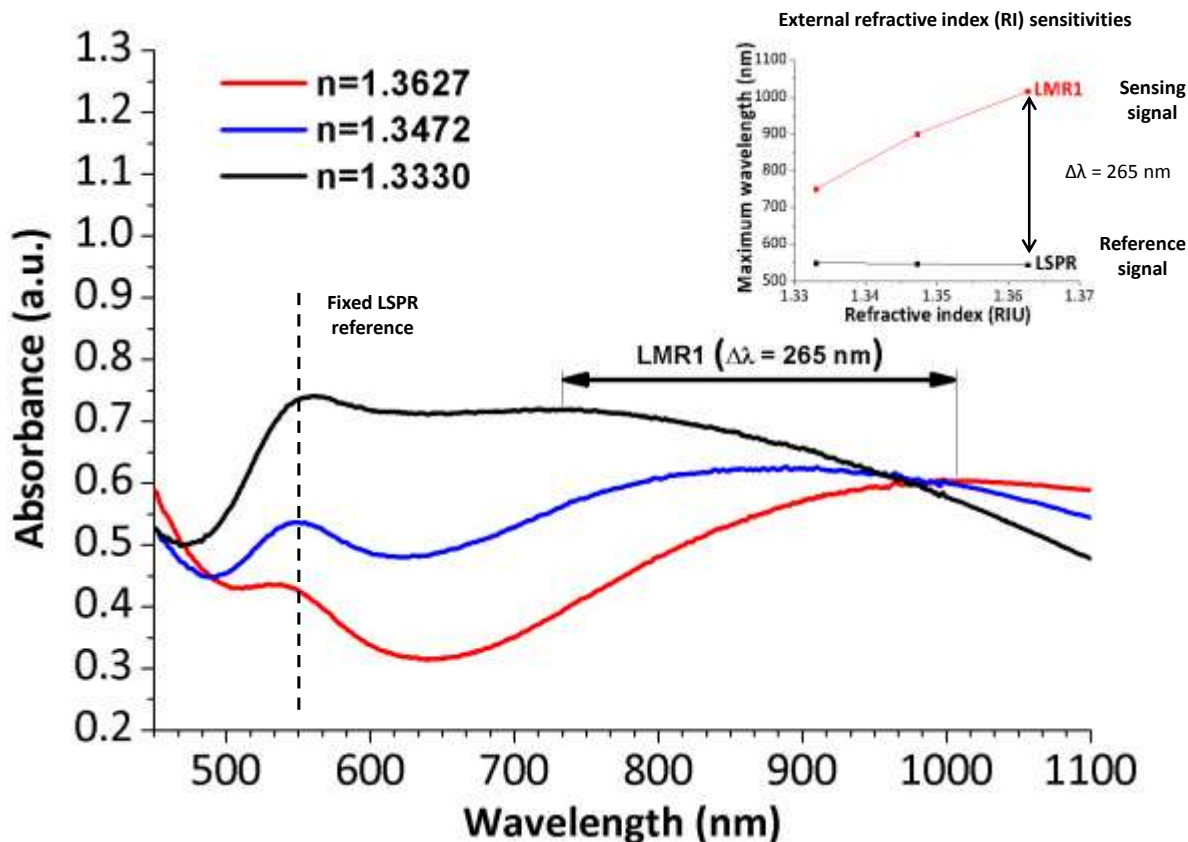
Figure 6. Spectral response of the LSPR (wavelength fixed reference) and LMR 1 (wavelength variation) absorption bands for 16-bilayers device when the sensitive region is immersed in different refractive indices from 1.3330 to 1.3627. The inset of the figure shows the great difference in sensitivities of both absorption bands to the external refractive index.

One of the main advantages of the design of this dual LSPR-LMR device is the possibility of fabricating self-referenced sensors. As we can see in the inset of the Figure 6, the LSPR band can be used as a reference signal (no variation in the wavelength position), whereas the LMR1 band can be used as a sensing signal to variations of the external refractive index.

c. Multi-LMR sensor (22-bilayers device)

The third device was fabricated by depositing 22 bilayers of [PAH(9.0)/PAA-AuNPs(9.0)] in order to make new LMR bands observable in the spectral range. For this specific number of bilayers, LMR1 is already out of the scope for this wavelength range, whereas LMR2 band remains in the visible range.

In Figure 7, it is possible to appreciate two new LMR absorption bands (LMR3 and LMR4) when the sensitive region is immersed in the water solution of glycerin with a refractive index value of 1.3627 and 1.4204, respectively. In addition, a red-shift of LMR peaks is observed, LMR2 and LMR3 respectively, as SMRI is increased. LMR2 is centered at 570 nm when the SMRI is 1.33 and is shifted to 935 nm when the SMRI is 1.4204. In a similar way, the LMR3 is shifted from 430 nm when the SMRI is 1.3627 to 540 nm when the SMRI is 1.4204. Attending to these results, the LMR2 shows a sensitivity of 4037 nm/RIU, whereas the LMR3 shows a sensitivity of 1906 nm/RIU. As we can see in Figure 7, the aspect of the LMR 2 and LMR 3 absorption bands are narrower than the LMR 1 absorption band (see Fig. 6).
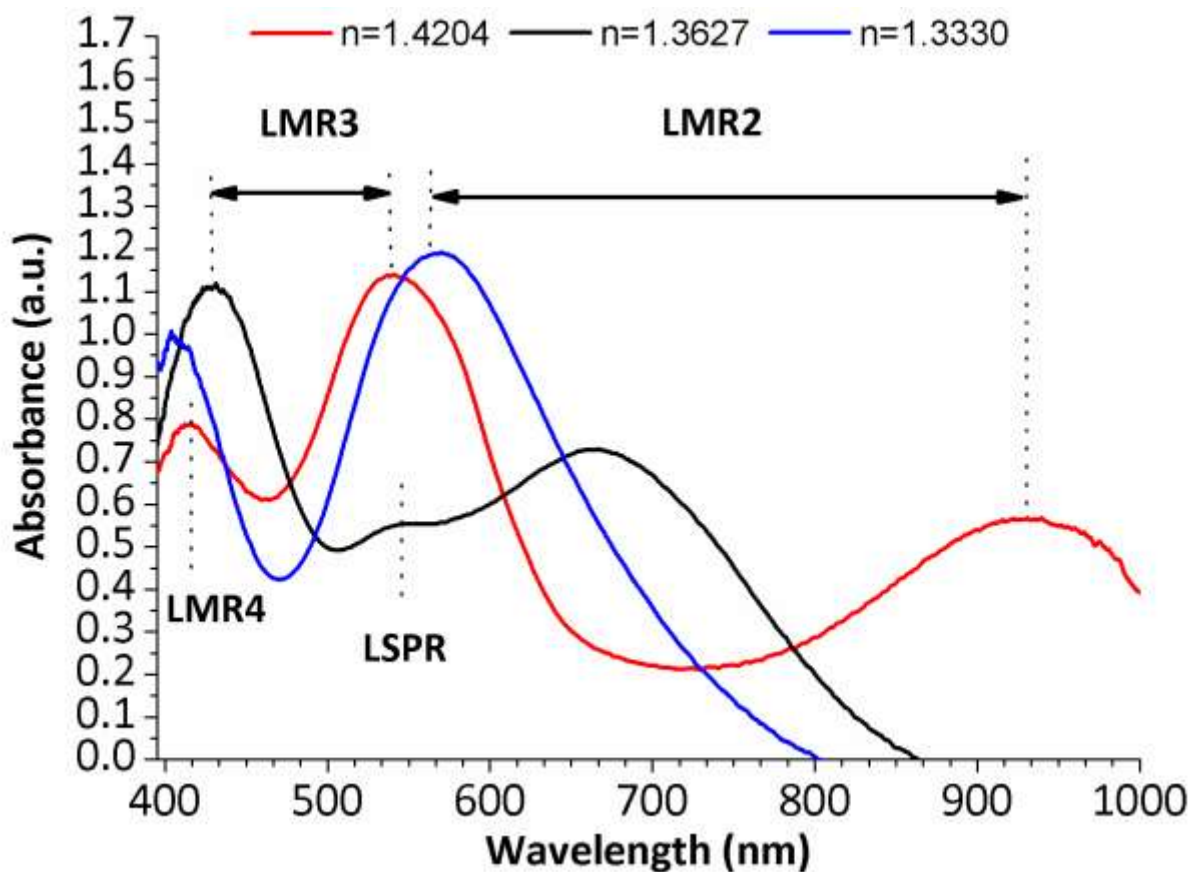

Figure 7. Spectral response of the LMR absorption bands (LMR2 y LMR3) for the 22-bilayers device when the sensitive region is immersed in different surrounding refractive indices.

In order to have a more precise idea of the different behavior in sensitivity related to the 22-bilayers device, Figure 8 shows the wavelength shift versus refractive index values of both

LMR2 and LMR3 bands. According to these results, the LMR2 shows more than two-fold increase in sensitivity than LMR3. The presence of this dual peak in a same device (22 bilayers) presents the additional advantage of more accurate measurements of the refractive index, showing a wavelength-based detection. Due to this, it is possible to estimate the SMRI as a function of the wavelength displacement of the both LMRs, and not only with the intensity shift of the LSPR. In Table 1, the main differences between the three fabricated devices are presented with their corresponding sensitivities.
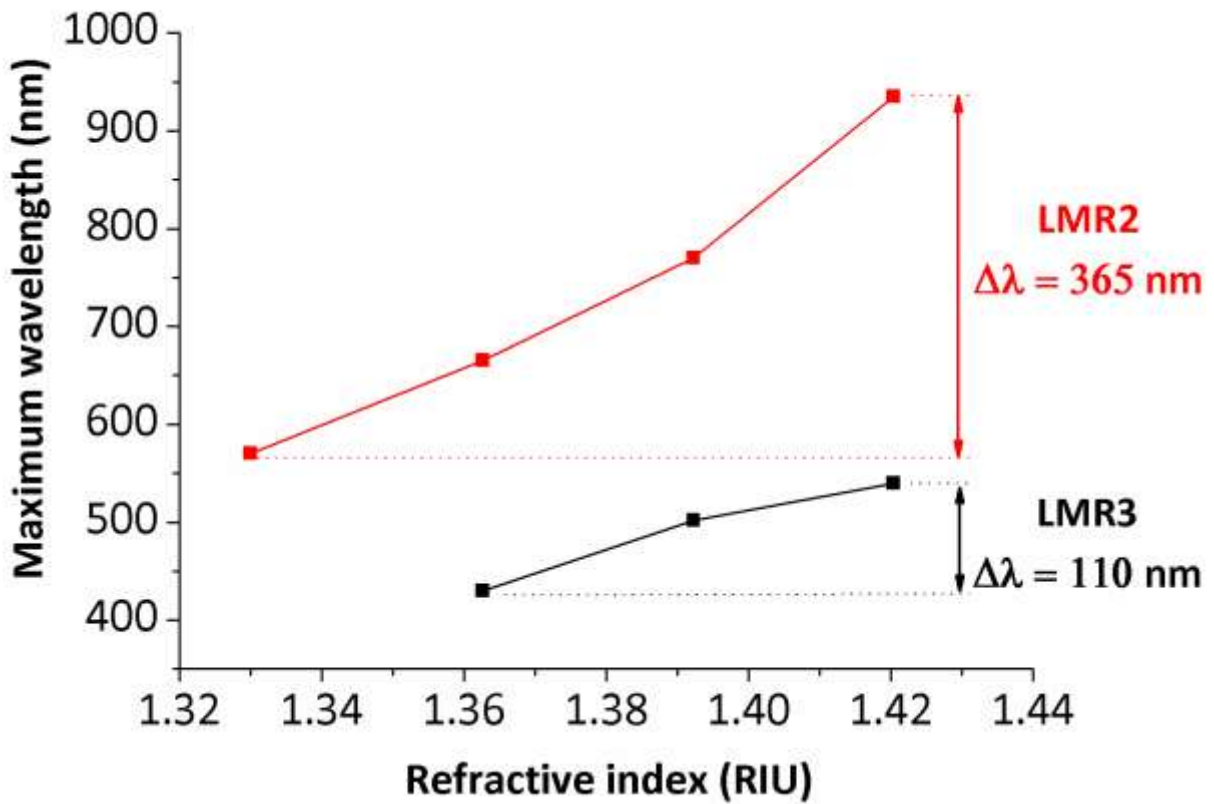

Figure 8. Experimental wavelength shift evolution of both LMR2 and LMR3 absorption bands to different surrounding refractive indices of the 22-bilayers device.

Table 1. A comparative table of the sensitivities (wavelength shift in nanometers versus refractive index unit) for the three devices analyzed.

Optical fiber device	Optical phenomenon	Sensitivity (nm/refractive index unit)
7-bilayers device	LSPR	Negligible
16-bilayers device	LSPR	Negligible
	LMR1	8922 nm/RIU
22-bilayers device	LMR2	4037 nm/RIU
	LMR3	1906 nm/RIU

Finally, and according to the experimental results, one of the most important advantages of using the LbL-E deposition technique is that the optical response of the sensors can be monitored during the fabrication process and it can be stopped at the moment when the LSPR, LSPR-LMR or multi-LMR bands are tuned to the desired wavelength position with their characteristic sensitivities.

IV.   CONCLUSIONS

In this work, three optical fiber devices based on different optical phenomena, LSPR, LSPR-LMR and multi-LMR absorption bands, have been fabricated and characterized for measuring the refractive index. The LbL-E deposition technique has been selected to fabricate the nanocoatings based on the successive incorporation of gold nanoparticles onto the uncladded core of a multimode optical fiber fragment. The transmitted spectra monitored during the deposition allow the study of the apparition and evolution of different absorption peaks as a function of the thickness coating.

The first device consists of a 7-bilayers coating and only the LSPR peak is observed which is centered at 530 nm, inherent to the gold nanoparticles. This peak remains at the same wavelength position during the whole fabrication process, showing only intensity variation without any wavelength dependence to the SMRI. The second device consists of 16-bilayers coating and two optical phenomena (LSPR and LMR1) at different wavelength positions are observed in the spectral range, showing a different behavior to the SMRI. The LSPR shows no significant wavelength dependence whereas LMR1 shows a strong wavelength response with a sensitivity of 8922 nm/RIU. And the third device consists of a 22-bilayers coating and multiple LMR peaks (LMR2, LMR3, LMR4) are observed when the sensitive coating is immersed in glycerin solutions with a variable refractive index value. The LMR2 and LMR3 peaks showed a sensitivity of 4037 and 1906 nm/RIU respectively. These results indicate that LMR2 improves the sensitivity in more than two times than LMR3. Finally, the presence of the LSPR peak in a same optical device can be used as a wavelength fixed reference, while LMR peaks can be used to measure the refractive index. To our knowledge, this is the first time that LSPR generated by gold nanoparticles and LMR peaks are simultaneously observed in a same device.

V. ACKNOWLEDGMENTS

REFERENCES

[1] P. R. Cooper, "Refractive-index measurements of liquids used in conjunction with optical fibers." Appl. Opt., vol. 22, pp. 3070-3072, 1983.

[2] M. Daimon and A. Masumura, "Measurement of the refractive index of distilled water from the near-infrared region to the ultraviolet region," Appl. Opt., vol. 46, pp. 3811-3820, 2007.

[3] M. Mitsushio, S. Higashi and M. Higo, "Construction and evaluation of a gold-deposited optical fiber sensor system for measurements of refractive indices of alcohols," Sens. Actuators A Phys, vol. 111, pp. 252-259, 2004.

[4] B. Culshaw and A. Kersey, "Fiber-optic sensing: a historical perspective", J. Lightwave Technol., vol. 26, pp. 1064-1068, 2008.

[5] Q. Wu, Y. Semenova, P. Wang and G. Farrell, "High sensitivity SMS fiber structure based refractometer – analysis and experiment," Opt. Exp., vol. 19, pp. 7937-7944, 2011.

[6] D. Jia, Z. Yao and C. Li, "The Transformer Winding Temperature Monitoring System Based on Fiber Bragg Grating," International Journal on Smart Sensing and Intelligent Systems, vol. 8, pp. 538-560, 2015.

[7] T. Wang, S. Korposh, S. James, R. Tatam and S. W. Lee, "Optical fibre long period grating sensor with a polyelectrolyte alternate thin film for gas sensing of amine odors," Sens. Actuators B, vol. 185, pp. 117-124, 2013.

[8] N. D. Rees, S. W. James, R.P. Tatam and G. J. Ashwell, "Optical fiber long-period gratings with Langmuir—Blodgett thin-film overlays", Opt. Lett., vol. 27, pp. 686-688, 2002.

[9] A. S. Guru Prasad, M. Anitha, K. S. Nanjunda Rao and S. Asokan "Measurement of Stress-Strain Response of a Rammed Earth Prism in Compression using Fiber Bragg Grating Sensors", International Journal on Smart Sensing and Intelligent Systems, vol. 4, pp. 376-387, 2011.

[10] L. Rindorf, J. B. Jensen, M. Dufva, L. H. Pedersen, P. E. Høiby and O. Bang "Photonic crystal fiber long-period gratings for biochemical sensing," Opt. Exp., vol. 14, pp. 8224-8231, 2006.

[11] Q. Sui, M. Jiang, Z. Jin, F. Zhang, Y. Cao and L. Jia, "Optical Fiber Relative Humidity Sensor Based on Fabry-Perot Interferometer Coated with Sodium-p-styrenesulfonate/allyamine Hydrochloride Films," Sensors and Materials, vol. 26, pp. 291-298, 2014.

[12] M. Yin, Q. An, J. Qian and A. Zhang, "Preparation and Application of Fiber-Optic Sensors Based on Layer-by-Layer Self-Assembly Multilayers," Progress in Chemistry, vol. 23, pp. 2568-2575, 2011.

[13] B. J. Luff, J. S. Wilkinson and G. Perrone, "Indium tin oxide overlayered waveguides for sensor applications," Appl. Opt., vol. 36, pp. 7066-7072, 1997.

[14] M. Yin, B. Gu, Q. Zhao, J. Qian, A. Zhang, Q. An, and S. He, "Highly Sensitive and Fast Responsive Fiber-Optic Modal Interferometric pH Sensor Based on Polyelectrolyte Complex and

Polyelectrolyte Self-Assembled Nanocoating," Analytical and Bioanalytical Chemistry, vol. 399, pp. 3623-3631, 2011.

[15] L. Bansal and M. A. El-Sherif, "1-5 Napthalenedisulphonic ACID Doped Polypyrrole Thin Films as Coatings to Optical Fibers for Organophosphate Sensing", International Journal on Smart Sensing and Intelligent Systems, vol. 3, pp. 230-252, 2010.

[16] M. Dashti, J. Mokhtari, M. Nouri and F. Shirini, "Imparting Conductivity and Chromic Behavior on Polyester Fibers by Means of Poly(3-Methylthiophene) Nanocoating," J Appl Polym Sci, vol. 124, pp. 3007-3012, 2012.

[17] M. Smietana, W. J. Bock, J. Szmidt and G. R. Pickrell "Nanocoating Enhanced Optical Fiber Sensors", Ceramic Transactions, vol. 222, pp. 275-286, 2010.

[18] P. J. Rivero, A. Urrutia, J. Goicoechea, I. R. Matias and F. J. Arregui, "A Lossy mode resonance optical sensor using silver nanoparticles-loaded films for monitoring human breathing," Sens. Actuators B, vol. 187, pp. 40-44, 2013.

[19] P. J. Rivero, M. Hernaez, J. Goicoechea, I. R. Matias and F. J. Arregui, "Optical fiber refractometers based on localized Surface plasmon resonance (LSPR) and lossy mode resonance (LMR)" Proc. SPIE 9157, 91574T, 2014.

[20] I. Del Villar, M. Hernaez, C. R. Zamarreño, P. Sánchez, C. Fernández-Valdivielso, F. J. Arregui and I. R. Matias, "Design rules for Lossy mode resonance based sensors," Appl. Opt., vol. 51, pp. 4298-4307, 2012.

[21] I. Del Villar, C. R. Zamarreño, M. Hernaez, F. J. Arregui and I. R. Matias, "Generation of lossy mode resonances with absorbing thin-films", J. Lightwave Technol., vol. 28, pp. 3351-3357, 2010.

[22] B. Liedberg, C. Nylander and I. Lunström, "Surface plasmon resonance for gas detection and biosensing," Sens. Actuators B, vol. 4, pp. 299-304, 1983.

[23] R. C. Jorgenson and S. S. Yee, "A fiber-optic chemical sensor based on surface plasmon resonance," Sens. Actuators B, vol. 12, pp. 213-220, 1993.

[24] Y. -. Kim, W. Peng, S. Banerji and K. S. Booksh, "Tapered fiber optic surface plasmon resonance sensor for analyses of vapor and liquid phases," Opt. Lett., vol. 30, pp. 2218-2220, 2005.

[25] L. Chau, Y. Lin, S. Cheng and T. Lin, "Fiber-optic chemical and biochemical probes based on Localized Surface Plasmon Resonance", Sens. Actuators B, vol. 113, pp. 100-105, 2006.

[26] Y. Shao, S. Xu, X. Zheng, Y. Wang and W. Xu, "Optical Fiber LSPR Biosensor Prepared by Gold Nanoparticle Assembly on Polyelectrolyte Multilayer", Sensors, vol. 10, pp. 3585-3596, 2010.

[27] S. K. Srivastava, V. Arora, S. Sapra and B. D. Gupta, "Localized Surface Plasmon Resonance-based fiber optic U-shaped biosensor for the detection of blood glucose," Plasmonics, vol. 7, pp. 261-268, 2012.

[28] M. Rycenga, C. M. Cobley, J. Zeng, W. Li, C. H. Moran, Q. Zhang, D. Qin and Y. Xia, "Controlling the synthesis and assembly of silver nanostructures for plasmonic applications," Chem. Rev., vol. 111, pp. 3669-3712, 2011.

[29] P. J. Rivero, A. Urrutia, J. Goicoechea, F. J. Arregui and I. R. Matías, "Humidity Sensor Based on Silver Nanoparticles Embedded in a Polymeric Coating", International Journal on Smart Sensing and Intelligent Systems, vol. 5, pp. 71-83, 2012.

[30] L. M. Liz-Marzán, "Nanometals: Formation and color", Materials Today, vol. 7, pp. 26-31, 2004.

[31] P. C. Angelomé, H. H. Mezerji, B. Goris, I. Pastoriza-Santos, J. Pérez-Juste, S. Bals and L. M. Liz-Marzán, "Seedless synthesis of single crystalline Au nanoparticles with unusual shapes and tunable LSPR in the Near-IR", Chem Mat, vol. 24, pp. 1393-1399, 2012.

[32] P. J. Rivero, J. Goicoechea, A. Urrutia and F. J. Arregui, "Effect of both protective and reducing agents in the synthesis of multicolor silver nanoparticles," Nanoscale. Res. Lett., vol. 8, pp. 1-9, 2013.

[33] Z. Wang, B. Tan, I. Hussain, N. Schaeffer, M. F. Wyatt, M. Brust and A. I. Cooper, "Design of polymeric stabilizers for size-controlled synthesis of monodisperse gold nanoparticles in water", Langmuir, vol. 23, pp. 885-895, 2007.

[34] G. Decher, "Fuzzy nanoassemblies: toward layered polymeric multicomposites," Science, vol. 277, pp. 1232-1237, 1997.

[35] P. J. Rivero, J. Goicoechea, I. R. Matias and F. J. Arregui, "A comparative study of two different approaches for the incorporation of silver nanoparticles into Layer-by-Layer films" Nanoscale Res. Lett., vol 9, pp. 1-11, 2014.

[36] P. J. Rivero, J. Goicoechea, A. Urrutia, I. R. Matias and F. J. Arregui, "Multicolor layer-by-layer films using weak polyelectrolyte assisted synthesis of silver nanoparticles" Nanoscale Res. Lett., vol8, pp. 1-10, 2013.

[37] P. J. Rivero, A. Urrutia, J. Goicoechea, and F. J. Arregui, "Optical fiber humidity sensors based on Localized Surface Plasmon Resonance (LSPR) and Lossy-mode resonance (LMR) in overlays loaded with silver nanoparticles", Sens. Actuators B, vol. 173, pp. 244-249, 2012.